Photochemistry and Photobiology, 2004, 80: 139–149

The Spatial Distribution of Optical Properties in the Ultraviolet and Visible in an Aquatic Ecosystem¶

Luca Bracchini,*[1] Steven Loiselle,[1] Arduino Massimo Dattilo,[1] Stefania Mazzuoli,[1] Andrés Cózar[1,2] and Claudio Rossi[1]

[1]Department of Chemical and Biosystems Sciences, University of Siena, Siena, Italy
[2]Area de Ecología, Facultad de Ciencias del Mar, University of Cadiz, Cádiz, Spain

Received 26 January 2004; accepted 13 May 2004

ABSTRACT

In aquatic ecosystems, the UV and visible radiation environment is strongly influenced by variation in the chemical and physical parameters of the ecosystems. In shallow lakes, highly heterogeneous water characteristics produce a wide variety of optical environments. Such ecosystems require analysis approaches that consider a potential variability. In this study, 77 stations were used to characterize the optical properties of a shallow lake (open water surface 54 km^2). The vertical attenuation of solar radiation at 305, 313, 320 and 340 nm and at photosynthetically active radiation was measured during the seasonal cycle. Dissolved organic matter (DOM), turbidity, fluorescence, pH, temperature, conductance and dissolved oxygen were simultaneously measured. The spatial variation of the extinction spectra of the dissolved fraction at each sampling station was also measured and analyzed between 270 and 400 nm. The spatial heterogeneity of the lake was examined by determining the distributions of the attenuation coefficients and biooptical parameters at high spatial resolution and describing the distributions in a series of maps. The methodology permitted a quantitative description of the interaction between solar radiation and aquatic ecosystems as well as a spatial classification of the dominating processes within the lake. This included the determination of the role played by DOM loading and changing chemical properties within the lake optical environment.

INTRODUCTION

The biological and chemical conditions of aquatic ecosystems are strongly influenced by the energy flux of solar radiation (J s^{-1}) and the interaction of this energy with the components of the system. The spectrum of solar radiation is subdivided into three bands: UV (290–400 nm), visible (400–700 nm) and IR (>700 nm). The UV radiation is divided into UV-B (290–320 nm) and UV-A (320–400 nm).

The study of interaction of solar energy in aquatic ecosystems has elicited a number of important research efforts (1–4). To characterize the fate of electromagnetic radiation within the medium, an attenuation coefficient (K_d, m^{-1}) is calculated based on the measurement of the downward irradiance flux at different depths. The attenuation coefficients can be calculated for one wavelength (spectral attenuation coefficient for downward irradiance, $K_{d,\lambda}$, m^{-1}) or for a specific band of spectra (attenuation coefficient for downward irradiance for a band of the spectra, $K_{d,\Delta\lambda}$, m^{-1}) (5).

The resultant attenuation coefficient will depend on the spatial and temporal variations of the chemical and physical characteristics of the environment. Besides the water itself, dissolved and particulate matter in the water column play an important role in the attenuation of UV and photosynthetically active radiation (PAR) radiation (6–8). The relationship between optical properties and water column components can be explored analyzing from a statistical point of view, using several aquatic ecosystems (9,10) or a single lake, if sufficient spatial resolution of sample station is chosen. Global scale maps representing an estimate of underwater UV radiation have been produced using remote sensing data (11). Nevertheless, this procedure does not provide a suitable resolution to assess spatial variations on the local scale (≤10 km).

Interest regarding the effect of UV radiation and its impact on the aquatic environment has increased in recent years. This is the result of an increase in available UV radiation in these ecosystems not only because of the reduction in the stratospheric ozone layer but also because of the modification of the aquatic environment in relation to local and regional pollution (12). The impacts of UV on the elements in trace quantities (13) as well as the abiotic and biotic communities (14–16) are reported to be potentially significant. Likewise, there is a well-documented relationship between changes in the chemical properties (*e.g.* pH and temperature) of aquatic ecosystems and UV penetration (17). Direct (18,19) and indirect (20) effects of UV radiation on nonliving and living systems have been the object of a number of important research efforts. In particular, the interaction of dissolved organic matter (DOM) with the UV and blue regions of the solar spectrum has been demonstrated (21–23). The dissolved matter photodegradation and photobleaching could reduce the ability of DOM to absorb UV radiation (24), and indirect photochemical production of free

¶Posted on the website on 28 March 2004

*To whom correspondence should be addressed: Department of Chemical and Biosystems Sciences, University of Siena, Via Aldo Moro 1, Siena, Si 53100, Italy. Fax: 39-0577-234177; e-mail: bracchini@unisi.it

Abbreviations: AU, arbitrary units; CB, central basin; CT, central station; DO, dissolved oxygen; DOM, dissolved organic matter; FA, fulvic acid; HA, humic acid; $K_{d,\Delta\lambda}$, attenuation coefficient for downward irradiance for a band of the spectra; $K_{d,\lambda}$, spectral attenuation coefficient for downward irradiance; NB, northern basin; NT, northern station; NTU, nephelometric turbidity unit; PAR, photosynthetically active radiation; SB, southern basin; SDK, Secchi disk; ST, southern station.

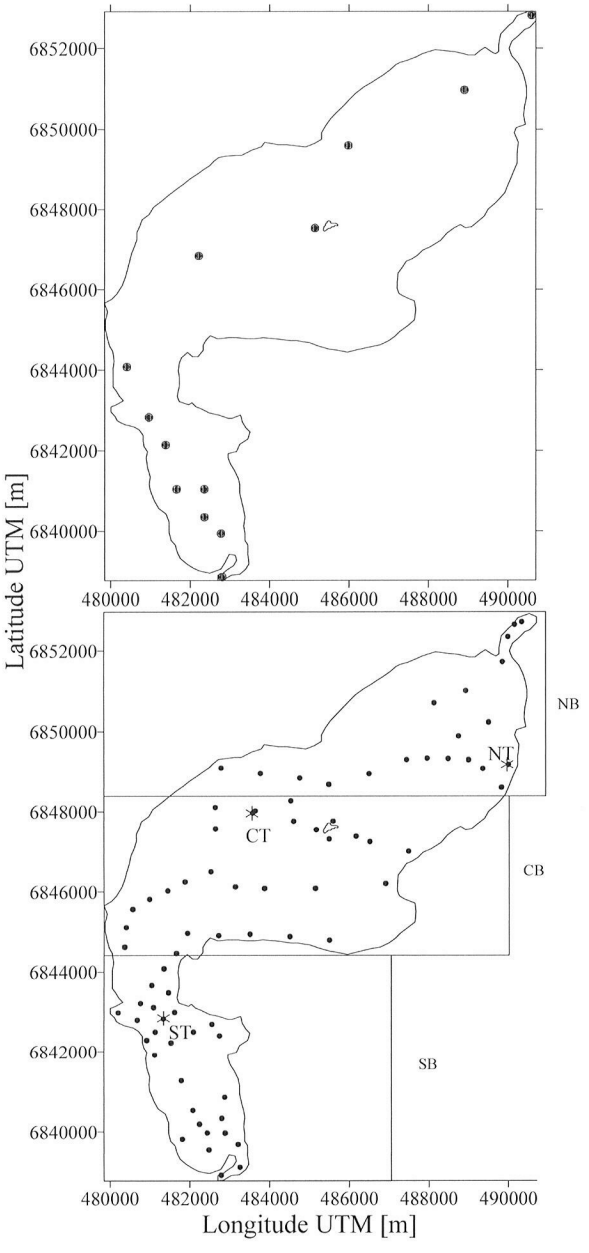

Figure 1. Distribution of measurements sampling stations during the first survey (13 stations) and the second survey (77 stations) in the Iberà Lake. The boxes denoted as SB, CB and NB show the geographical division of the Iberà Lake into southern, central and northern basins, respectively. The asterisks represent the southern station (ST), central station (CT) and northern station (NT).

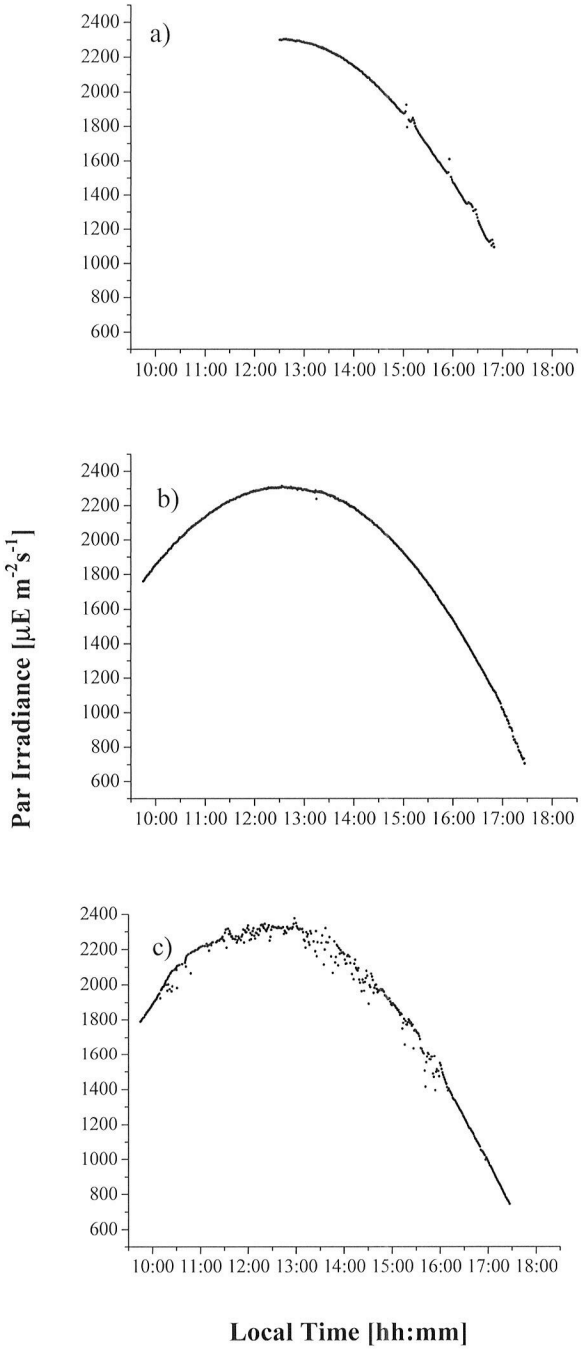

Figure 2. Measured PAR irradiance at the water surface on (a) 30 October 2001, (b) 31 October 2001 and (c) 1 November 2001.

radicals is potentially harmful to the plankton community (25–27). In this study, local-scale changes of the environment light field were studied in relation to changes in the chemical properties of aquatic ecosystem with the help of high-resolution maps representing the measurements. The maps were used to evaluate the ecological aspects of the studied ecosystem, such as the influence of inflowing rivers on the optical properties of the lake.

MATERIALS AND METHODS

Study site. This study was conducted in the Esteros del Iberà wetland in northeast Argentina and in particular in the Iberà Lake, which is located at 28° south and 57° west. The study site is a Ramsar wetland of international importance and is characterized by a significant biodiversity (28).

The Iberà Lake (open water area 54 km^2) is a permanent lake with an average depth of 3 m and a maximum of 4.5 m. The lake has two small rivers, which drain wetland areas into the southern and northern parts of the lake. The lake border consists of floating vegetation mats. These mats extend up to 1 km in width and 2 m in depth and consist of living vegetation in a substrate of degraded plant matter that is in contact with the water below and on each side. Organic matter and humic substances are constantly being released by the vegetation mats into the surrounding water.

The measurements were made in two campaigns in the same year, the first on 27 April 2001 (austral autumn) and the second on 30 October 2001, 31 October 2001 and 1 November 2001 (austral spring). In the first survey, measurements were made in 13 stations in the lake, whereas in the second

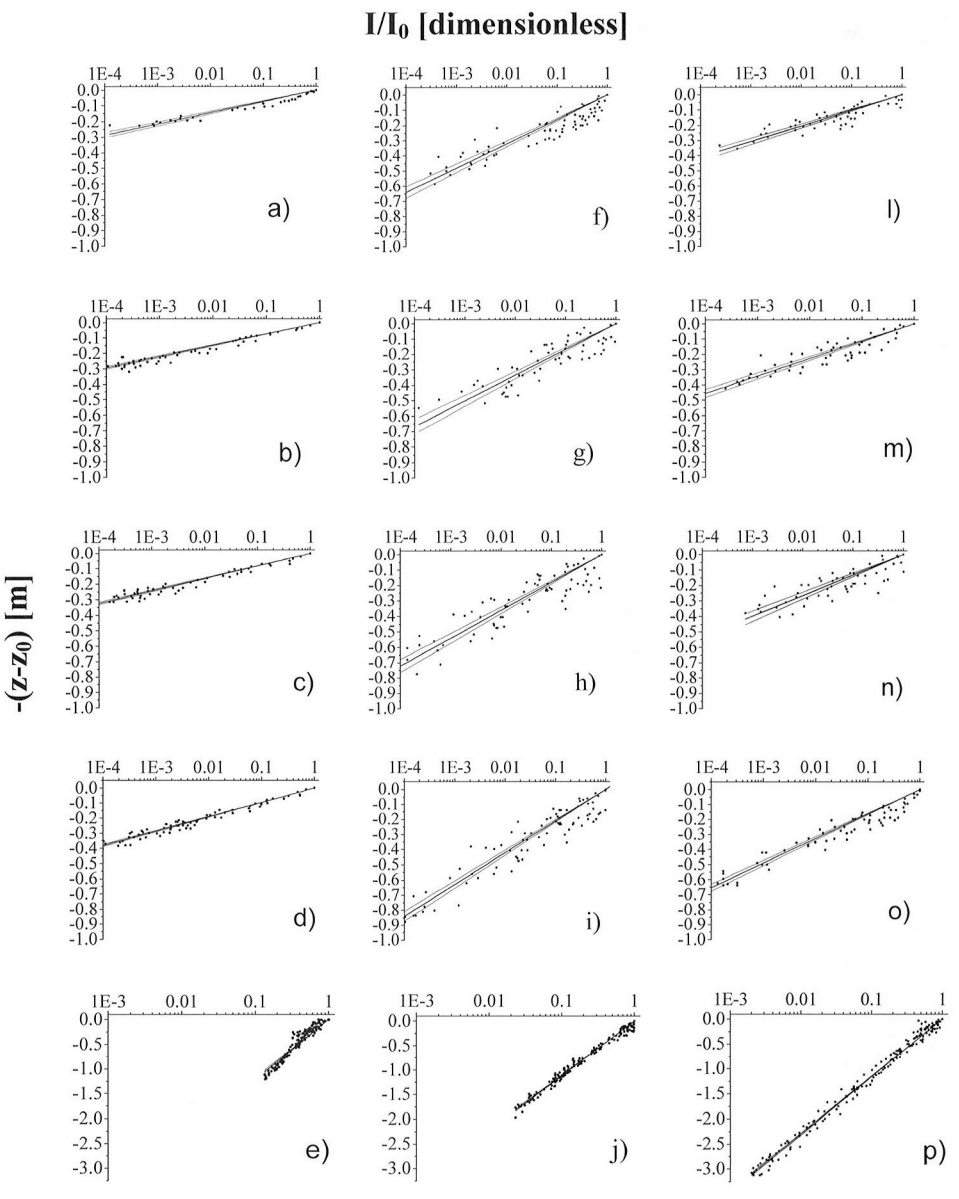

Figure 3. Measured profile ratio for 305, 313, 320 and 340 nm and PAR irradiance for three stations with depth: NT (a–e), CT (f–j) and ST (l–p). The best linear fit (bold line) and the 95% confidence band (fine lines) are presented.

survey 77 stations were used (Fig. 1). Each day, transects were performed throughout the lake. Measurements were made between 1030 and 1530 h (local time) on days with limited cloudiness and low wind conditions. The abovesurface solar irradiance was measured in the second campaign using a PAR sensor (SKP SN 210010121977 calibrated on 19 January 2001, Skye Instruments Ltd., Llendrindod Wells, UK) (Fig. 2). Unfortunately, the PAR sensor failed during the day of the autumn measurements (the incident PAR irradiance was measured in $\mu E\ m^{-2}\ s^{-1}$).

In each station, a vertical profile of the UV and PAR irradiance was measured using a PUV541 spectroradiometer SN 19235 (Biospherical Instruments, San Diego, CA). The instrument was calibrated in March and July 2001 by comparing the measured irradiances of the instrument with a second spectroradiometer (SUV-100, Biospherical Instruments) with a spectral resolution of 1 nm. The spectral irradiance ($\mu W\ cm^{-2}\ nm^{-1}$) channels in the UV band of the PUV541 were 305 nm (band-pass 7 nm), 313 nm (band-pass 10 nm), 320 nm (band-pass 11 nm) and 340 nm (band-pass 10 nm), with a cosine response. The dark current signal of the sensor, expressed in spectral irradiance units, was of the order of 0.001 $\mu W\ cm^{-2}\ nm^{-1}$ or less.

During the measurements in the lake, the PUV541 was connected to a portable battery and a portable computer to collect the irradiance data. The instrument was lowered into the water column, and measurements of UV and PAR radiation, water temperature and water depth were acquired simultaneously every 0.3 s. The irradiance measurements were initiated below the waterline (0.02 m) and were recorded while the instrument was lowered to the lake bottom as well as during the raising of the instrument to below the water surface. On average, 60 measurements (irradiances, temperature [°C] and water depth [m]) were obtained in each profile.

The resulting radiation profile was corrected by removing the dark current signal and plotted against the water depth. The attenuation coefficient was calculated by fitting the best exponential curve to the profile data for each wavelength, following Eq. 1.

$$I_\lambda = I_{0,\lambda} \exp(-K_{d,\lambda}(z - z_0)) \quad (1)$$

where z is water depth, z_0 is 0.02 m, $I_{0,\lambda}$ is the irradiance at 0.02 m and $K_{d,\lambda}$ is the spectral attenuation coefficient for the downward solar radiation at λ. An analogous procedure was used for the PAR measurements ($\mu E\ m^{-2}\ s^{-1}$) substituting the wavelength λ with $\Delta\lambda$ = par. The profile representation was determined using a linear regression following modification of Eq. 1:

$$-\frac{K_{d,\lambda}}{2.303}(z - z_0) = \log\left(\frac{I_\lambda}{I_{0,\lambda}}\right) \quad (2)$$

During each profile, a sample at 0.30 m depth was obtained and measurements of turbidity (nephelometric turbidity unit [NTU]) and *in vivo*

Table 1. Estimated attenuation coefficients for UV and PAR radiation in the ST, CT and NT based on November 2001 data in the Iberà Lake represented in Fig. 3. SD represents the standard deviation of the estimated attenuation coefficient

	ST	R^2	CT	R^2	NT	R^2
$K_{d,305}$ (m^{-1})	22.6	0.75	14.3	0.77	32.1	0.91
SD $K_{d,305}$ (m^{-1})	0.8		0.4		0.9	
$K_{d,313}$ (m^{-1})	20.2	0.81	13.8	0.71	31.3	0.91
SD $K_{d,313}$ (m^{-1})	0.6		0.5		0.5	
$K_{d,320}$ (m^{-1})	17.3	0.62	12.8	0.78	28.3	0.93
SD $K_{d,320}$ (m^{-1})	0.7		0.4		0.4	
$K_{d,340}$ (m^{-1})	14.1	0.92	11.0	0.90	24.1	0.96
SD $K_{d,340}$ (m^{-1})	0.3		0.2		0.2	
$K_{d,par}$ (m^{-1})	2.001	0.99	2.07	0.98	1.91	0.90
SD $K_{d,par}$ (m^{-1})	0.009		0.01		0.03	

natural fluorescence (arbitrary units [AU]; optics: photodiodes; excitation wavelength, 460 nm; detector wavelength, 685 nm) were made using a Scufa II Fluorometer (Self-Contained Underwater Fluorescence Apparatus, Turner Designs, Sunnyvale, CA). The turbidity channel was calibrated using a Formazin Turbidity Standard Solution (Hach Company, Loveland, CO) diluted in Milli-Q water to obtain a solution of 30 NTU. The natural fluorescence channel was set to measure in a range from 0 AU (corresponding with an analog output of 0 V) to 500 AU (corresponding with an analog output of 5 V). The stability of the fluorometer channel was checked, in each station, with a solid secondary standard (Turner Designs). A temperature compensation algorithm for fluorescence measurements (linear compensation coefficient 1.4% per °C) was used. Temperature (°C), dissolved oxygen (DO) (mg L^{-1} and percentage of saturation value), pH and conductibility (μS cm^{-1}) were measured with the multiprobe Datasonde 3 (Hydrolab Corporation, Austin, TX). All sensors, except the temperature sensor, were calibrated each day. The Datasonde 3 was submersed with the sensors at 0.30 m below water surface. The probe was programmed to collect measurements every 10 s. The average values of measurements were collected and reported.

At each sampling station, a sample of water was collected and filtered *in situ* with a 0.22 μm single-use filter (Millex GP Filter Unit, Millipore SA, Molsheim, France). The samples were preserved in the dark at 4°C until the spectrophotometric analysis. The absorbance (cm^{-1}) of the dissolved matter (measured at 272 nm and between 270 and 400 nm) in each filtered sample was measured using an Ultrospec 2000 spectrophotometer (Pharmacia Biotech, Buckinghamshire, England) using a quartz cuvette and a blank of Milli-Q water. After acclimatization in a temperature-controlled room (18°C), the absorbance was measured with a spectral resolution of 1 nm. Absorbance at 272 nm was used to measure the concentration of DOM.

The stock solution of DOM was prepared by dissolving 25 mg of humic acid (HA) sodium salt standard (Sigma–Aldrich Chemie, Gmbh, Munich, Germany) in 5 mL of 0.1 *M* NaOH solution, followed by sonication, pH adjustment to 7 and dilution with Milli-Q water to 50 mL. The stock solution (500 ppm) was filtered through a 0.22 μm pore diameter Millipore membrane and stored at 4°C in the dark (29). The effective concentration of the stock solution was determined by gravimetric measurement. The calibration line was performed using stock solution with concentration between 0 and 20 mg L^{-1}.

The 0.22 μm filtered stock solution was also analyzed to determine the distribution of the molecular weight of the DOM present in solution using Centrifugal Filter Devices (Amicon bioseparations, Millipore Corp., Bedford, MA). After separation by centrifugation, the absorbance at 272 nm was used to determine the molecular weight of each fraction. The stock solution was found to contain 49% HA (>30 000 Da), 12% fulvic acid (FA) (5000–30 000 Da) and 39% lower molecular weight DOM (<5000 Da). Therefore, the calibration curve developed with stock HA solution was considered an appropriate standard for measurements of the range of DOM molecular weights found in the study lake (30).

The wavelength of 272 nm was selected because it supplies an estimation of all DOM present and is linked to the concentration of aromatic ring structures. The wavelength of 272 nm is also used in aromaticity studies for the characterization of aquatic organic solutes (31–33).

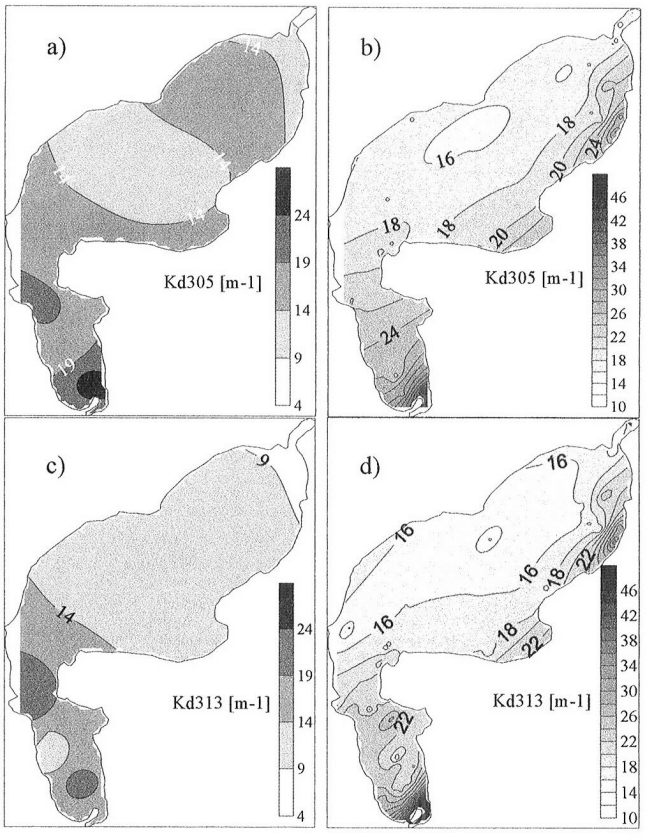

Figure 4. Spatial distribution of (a) $K_{d,305}$ (number of station used, N = 12) and (c) $K_{d,313}$ (N = 12) for the autumn survey. Spatial distribution of (b) $K_{d,305}$ (N = 54) and (d) $K_{d,313}$ (N = 73) for the spring survey.

The absorbance spectrum (measured between 270 and 400 nm) that results from the spectrophotometric analysis of the filtered water samples was used to determine changes in the molecular structure of the dissolved matter within the lake. The slope of the exponential decrease in absorbance with increasing wavelength was analyzed according to the analysis proposed by Bricaud *et al.* (34) with the introduction of a background parameter (γ, cm^{-1}) according to Eq. 3 (35,36):

$$a(\lambda) = a(\lambda_0)e^{s(\lambda_0-\lambda)} + \gamma \quad \text{with } 270\,\text{nm} \leq \lambda \leq 400\,\text{nm} \qquad (3)$$

where λ_0 = 290 nm, $a(\lambda_0)$ is the measured absorbance at 290 nm, s (nm^{-1}) is the slope of the spectra and γ is an additional background parameter.

To examine the spatial distribution of the optical and biooptical lake measurements, maps were created using the Surfer 7.0 software and the Kriging interpolation method. Likewise, maps of the standard deviation were also determined but are not shown here. The values of standard deviation were used to determine the number of classes used in the spatial representation (maps) of the optical and biooptical measurements. The class interval was chosen to be equal to or greater than the maximum standard deviation. The boundary of the lake was determined using a georeferenced satellite image (Band 4, Landsat 7) (projection: Gauss Kruger; spheroid: WGS84; coordinate system: UTM, m).

RESULTS AND DISCUSSION

The measured irradiance profiles and the attenuation coefficients for each station were obtained using Eq. 2. Measured and fitted profiles for UV and PAR irradiances are presented for three different stations in the lake, in the northern (NT), the central (CT) and the southern sections (ST) for the spring survey (Fig. 3).

In these three stations, the depth to which 1% of the surface irradiance at 305 nm penetrates was measured to be 0.20, 0.32 and

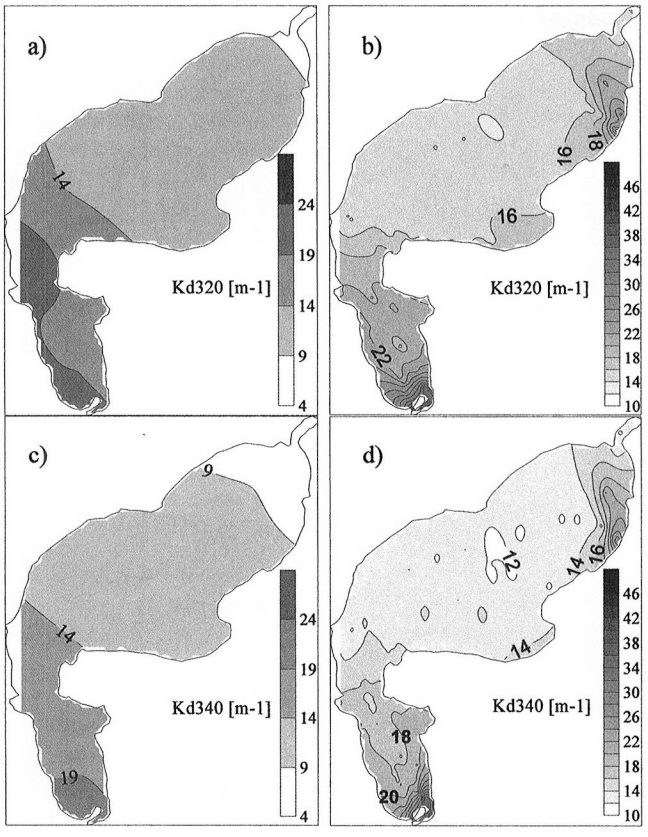

Figure 5. Spatial distribution of (a) $K_{d,320}$ (N = 12) and (c) $K_{d,340}$ (N = 12) for the autumn survey. Spatial distribution of (b) $K_{d,320}$ (N = 75) and (d) $K_{d,340}$ (N = 76) for the spring survey.

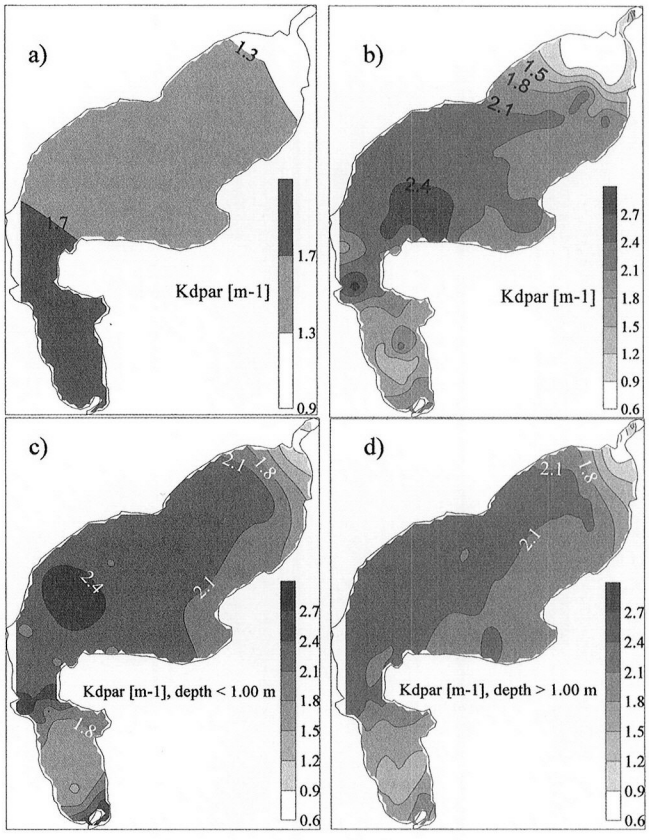

Figure 6. Spatial distribution of $K_{d,par}$ for the (a) autumn survey (N = 13) and (b) spring survey (N = 77). Spatial distribution of $K_{d,par}$ measured (c) before 1.00 m and (d) below 1.00 m during the spring survey.

0.14 m in southern, central and northern area, respectively. The penetration depth for 313 nm irradiance for the three stations was 0.23, 0.34 and 0.15 m. For 320 nm, the 1% depth was found to be 0.27, 0.36 and 0.16 m. For 340 nm, the depths were 0.32, 0.40 and 0.20 m. Considering data from all stations in both sampling surveys, UV is not measurable beyond a depth of 1.00 m (measured with PUV541 instrument at $\lambda \leq 340$ nm).

The depth to which 1% of surface PAR irradiance was measured was 2.25 m at the ST, whereas there was more than 1% of surface irradiance of PAR at the lake bottom in the other two stations.

The attenuation coefficient in the three stations shows significant differences among stations (Table 1).

To better examine the spatial distribution of the optical measurements, the georeferenced data were used to create a series of maps.

Twelve stations were used for the autumn spatial analysis, whereas a maximum number of 76 stations were used for the spring campaign (Figs. 4 and 5). In the autumn survey, the 305 nm attenuation coefficient (Fig. 4a) was measured to be between 14 and 24 m^{-1} in the southern basin (SB), whereas $K_{d,305}$ in the central and northern basins (CB and NB, respectively) was found to be much lower, between 4 and 14 m^{-1}. At areas far from the sampling stations, the maximum value of the standard deviation was 5 m^{-1}, which is high but sufficient to allow for the geographical distribution of the $K_{d,305}$.

The same structural spatial variation was observed during the spring survey (Fig. 4b) with the exception of the northeastern part of the lake where a relative maximum of the 305 nm attenuation coefficient was observed. In the SB, during the spring, values between 48 m^{-1} (the absolute maximum) and 20 m^{-1} were measured. In the CB and NB, values between 18 and 20 m^{-1} were measured. In the eastern side of the CB and NB (near the shore of the lake), attenuation coefficients between 20 and 30 m^{-1} were measured. In the CB and NB, the attenuation coefficients were more homogeneous with respect to the SB measured values. The maximum value of the standard deviation of the spring measurements was 0.9 m^{-1}. During spring, the attenuation measurements at 305 nm are significantly higher than during autumn.

Similar results were found for the distribution of $K_{d,313}$, $K_{d,320}$ and $K_{d,340}$ in the two surveys. Using the same methodology, $K_{d,par}$ maps were created (Fig. 6a,c).

During the autumn measurement, $K_{d,par}$ values in the SB (1.7 $m^{-1} \leq K_{d,par} \leq 1.9$ m^{-1}) were higher with respect to both the NB (0.9 $m^{-1} \leq K_{d,par} \leq 1.4$ m^{-1}) and the CB (1.4 $m^{-1} \leq K_{d,par} \leq 1.8$ m^{-1}) (Fig. 6a). The maximum value of standard deviation in the autumn survey was 0.4 m^{-1}. In the spring campaign (Fig. 6b), the highest values were observed in the CB (2.4 $m^{-1} \leq K_{d,par} \leq 2.7$ m^{-1}) in comparison with the SB (1.4 $m^{-1} \leq K_{d,par} \leq 2.4$ m^{-1}) or NB (0.6 $m^{-1} \leq K_{d,par} \leq 1.4$ m^{-1}). The maximum value of standard deviation in the spring survey was 0.3 m^{-1}. In the CB, the $K_{d,par}$ values were higher in spring than in autumn, whereas this trend was reversed in the SB and NB.

To examine the possibility of an optical stratification of the water column, PAR attenuation coefficients were calculated above and below 1.00 m depth (spring survey, Fig. 6c,d). The distributions of the $K_{d,par}$ above and below 1.00 m show strati-

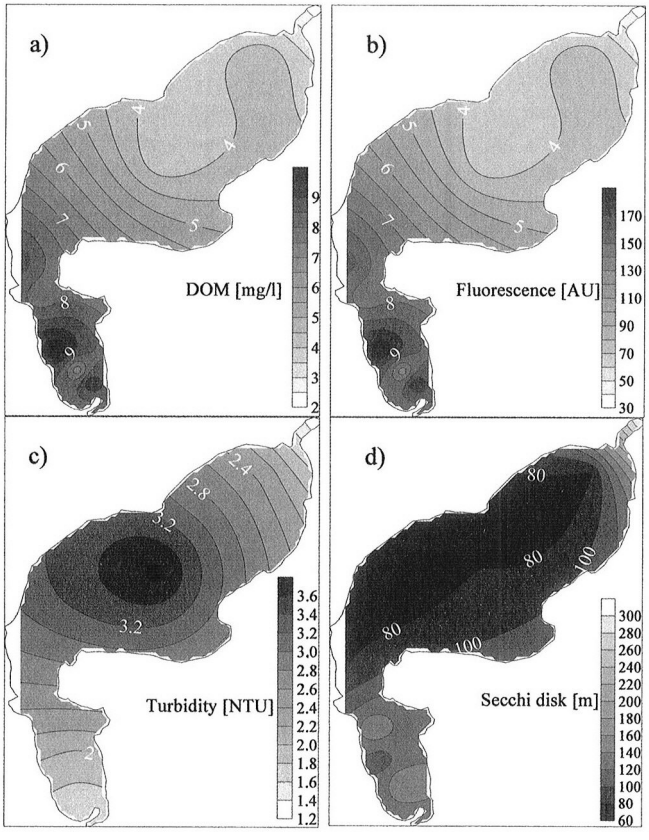

Figure 7. Qualitative spatial distribution of the (a) DOM, (b) fluorescence, (c) turbidity and (d) SDK depth measured during the autumn season.

fication in small areas of the lake (central part of SB and western part of CB), with difference in the PAR attenuation coefficient of less than 0.5 m^{-1}. The northern part of NB was the area with a lower optical stratification. The PAR attenuation coefficient was higher in the first meter of the water column than in the remainder of the water column.

The distribution of DOM, fluorescence, turbidity and Secchi disk (SDK) depth (for the first campaign only) are presented in Fig. 7 (a–d, respectively) and Fig. 8 (a–c). In the spring campaign, 77 stations were used to calculate the maps and the standard deviation. During autumn, maps of the standard deviation cannot be calculated because of the limited number of measurement stations. In this case, the maps represent only the qualitative trends, in particular in areas that were far from the measurement stations.

The DOM was higher in the SB than in the CB and NB for both surveys, and there is no appreciable difference between the absolute values measured during the autumn and spring seasons. The turbidity measurements were highest in the CB, with minimum values in SB and NB for both campaigns. The absolute values were higher during the spring season with respect to the autumn season. The fluorescence measurements in the autumn survey were lowest (60–140 AU) in the SB with a maximum in the CB and NB ($\geq$180 AU). The fluorescence of the spring survey was maximum in the CB ($\geq$450 AU) and minimum in the NB ($\leq$50 AU).

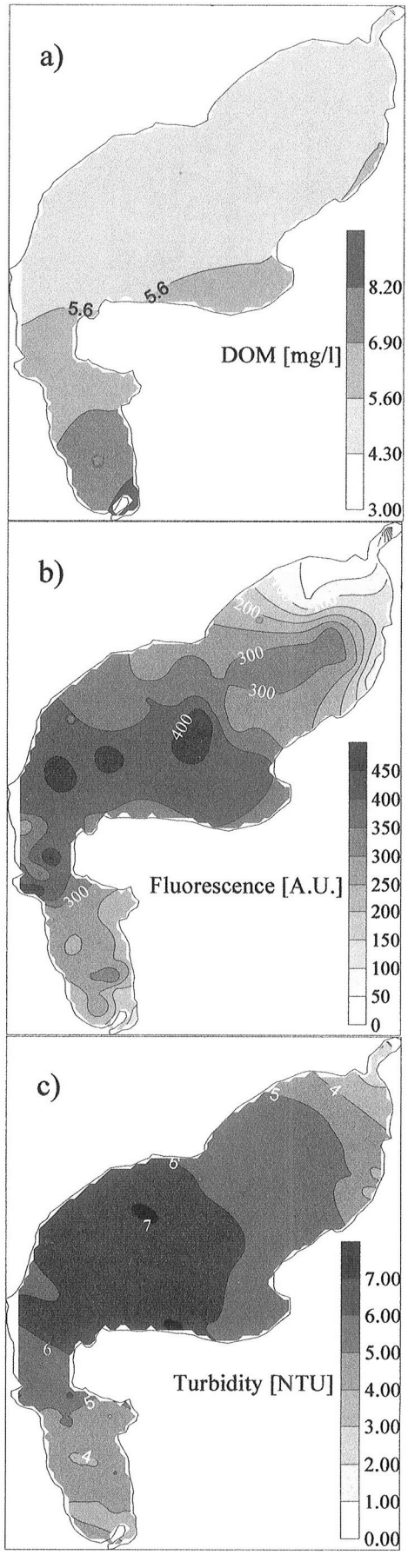

Figure 8. Spatial distribution of the (a) DOM, (b) fluorescence and (c) turbidity measured during the spring season.

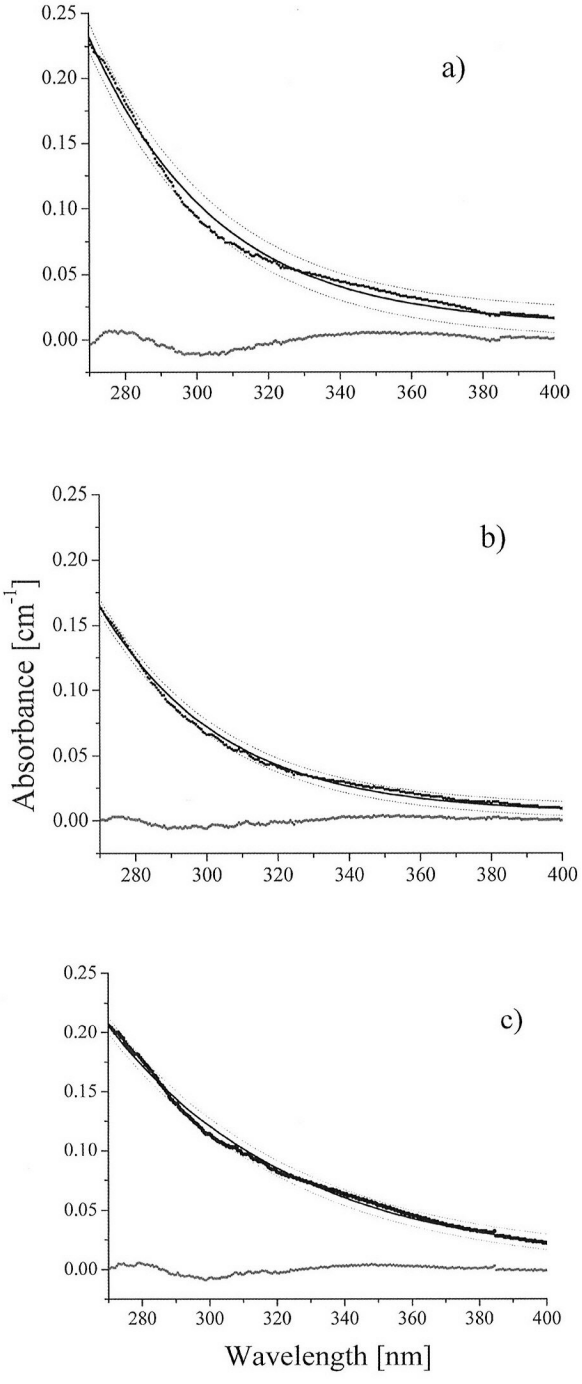

Figure 9. Absorption spectra (decadic values) of the 0.22 μm filtered water sample for three stations (a) ST, (b) CT and (c) NT after subtraction of the Milli-Q water blank. The residual curve, between the best fit and the data, and the 99.9% confidence band are presented. The observed residuals (40% of samples) may be interpreted, consistent with Stedmon *et al.* (36), with the origin of DOM and the littoral area characteristics. Data from spring survey.

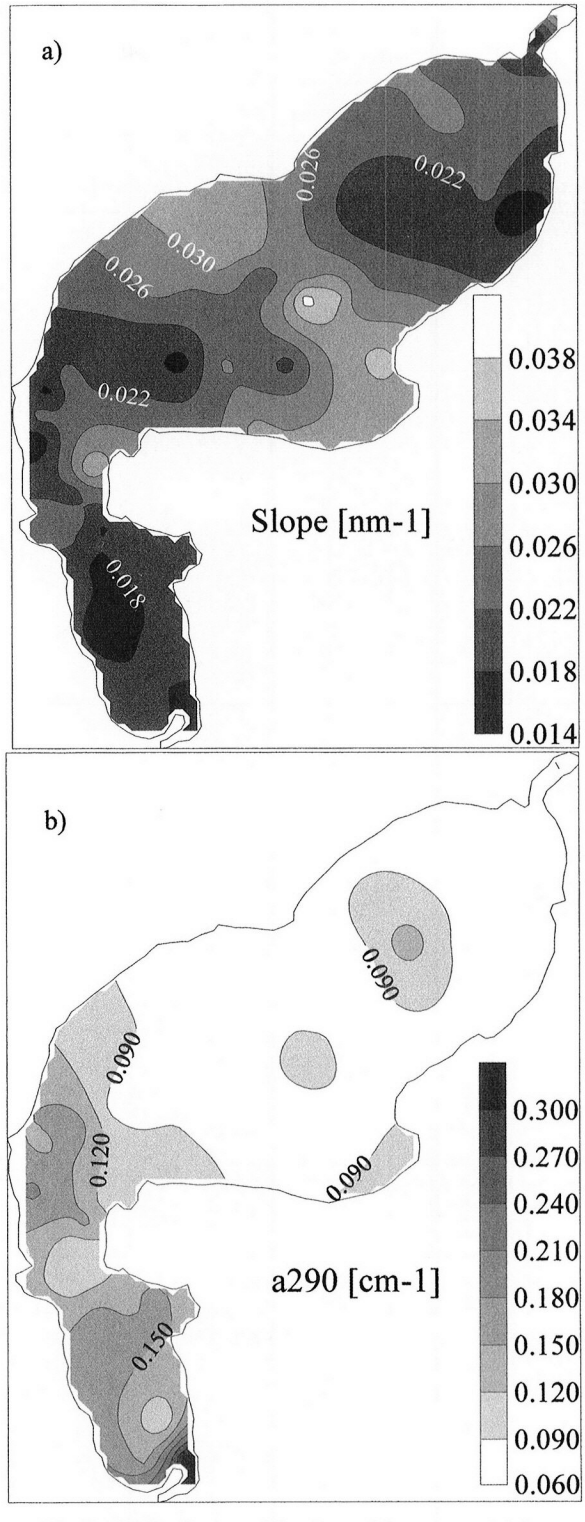

Figure 10. Spatial distribution of the slope of the exponential decrease in absorbance in (a) wavelength 270–400 nm and (b) $a(\lambda_0 = 290)$ (decadic values). Data from spring survey.

The data of the spectrophotometric analysis of the filtered water sample (DOM fraction) are presented for the three stations (Fig. 9: [a] ST, [b] CT [c] NT) in the spring campaign together with the fitted exponential curve Eq. 3 to determine the slope from 270 to 400 nm. The residuals between the theoretical exponential curve and measured absorbance are also presented (gray curves in Fig. 9a–c).

The spectral properties of DOM were analyzed in accordance with the three subdivision of the lake. The averages and the standard deviations of $a(\lambda_0)$ and slope were calculated. The standard deviation value represents not so much the uncertainty in the measurements as the spatial variation in each basin. For the SB,

Table 2. Physical and chemical measurements of the SB of Iberà Lake in November 2001. The last two rows report the average and standard deviation (SD) of measurements

Southern basin						
Station	T ± 0.2 (°C)	pH ± 0.2	DO (%)	DO ± 0.2 (mg L^{-1})	C ± 0.2 (µS cm^{-1})	SDK ± 0.05 (m)
4						1.25
5						1.00
7						1.10
10						1.00
11						1.25
16						0.75
17						1.75
18						0.75
20						1.00
61						0.85
62	24.0	6.7	101.0	8.5	14.2	0.90
63	24.0	6.6	99.3	8.4	14.5	1.60
64	23.9	6.6	98.4	8.3	14.8	1.60
65	24.0	6.7	102.0	9.8	14.6	1.60
66	24.3	6.7	101.0	8.4	14.2	1.60
67	23.9	6.4	100.0	8.5	14.6	1.50
68	23.9	6.5	100.0	8.4	14.7	1.50
Average	24.0	6.6	100	8.6	14.5	1.2
SD	0.2	0.1	1	0.5	0.2	0.3

the value was found to be 0.16 ± 0.05 (base 10 logarithm absorption, cm^{-1}), whereas similar average values were found for the CB and NB (0.09 ± 0.02 cm^{-1} and 0.08 ± 0.02 cm^{-1}, respectively). (Note that the absorbance is measured with base 10 logarithm. To obtain the Napierian logarithmic base values of absorbance, it is sufficient to multiply by 2.303 the decadic absorbance.) The average value of the slope in the SB was 0.020 ± 0.004 nm^{-1}. In the CB, the average value of the slope was 0.029 ± 0.006 nm^{-1}, whereas in the NB, the average value was 0.023 ± 0.005 nm^{-1}. No differences were found in the γ parameter (0.004 ± 0.002 cm^{-1} for all basins). To better understand the

Table 3. Physical and chemical measurements of the CB of Iberà Lake in November 2001. The last two rows report the average and standard deviation (SD) of measurements

Central basin						
Station	T ± 0.2 (°C)	pH ± 0.2	DO (%)	DO ± 0.2 (mg L^{-1})	C ± 0.2 (µS cm^{-1})	SDK ± 0.05 (m)
21						1.00
23						1.00
28						0.80
32						0.85
36						0.75
70	23.9	8.0	106.8	9.0	12.5	0.75
71	24.0	8.1	108.1	9.1	12.4	0.75
72	24.0	8.1	106.5	9.0	12.3	0.75
73	24.0	7.9	106.3	9.0	12.6	0.75
74	24.4	7.3	104.1	8.7	12.2	0.75
75	24.3	8.1	107.6	9.0	12.0	0.75
76	24.2	8.6	108.4	9.1	12.7	0.75
77	24.3	8.5	107.5	9.0	12.8	0.85
Average	24.1	8.1	107	9.0	12.4	0.8
SD	0.2	0.4	1	0.1	0.3	0.1

Table 4. Physical and chemical measurements of the NB of Iberà Lake in November 2001. The spatial distance of Stations 41 and 42 was less than 50 m. These stations were located in the north small river and the measures were collected on 2 different days. The same description is valid for Stations 43–46. The last two rows report the average and standard deviation of measurements. The averages and standard deviation values calculated without Stations 41–46 are presented in parentheses.

Northern basin						
Station	T ± 0.2 (°C)	pH ± 0.2	DO (%)	DO ± 0.2 (mg L^{-1})	C ± 0.2 (µS cm^{-1})	SDK ± 0.05 (m)
41	24.9	5.8	64.0	5.3	15.0	0.75
42	24.8	5.8	60.4	5.0	15.0	1.10
43	24.6	5.8	70.3	5.9	14.8	4.00
44	25.0	5.9	78.9	6.5	14.2	4.00
45	25.2	5.9	81.1	6.7	14.8	4.00
46	25.0	5.9	80.7	6.7	14.2	4.00
47	24.8	7.0	98.2	8.1	12.2	4.00
48	24.5	8.2	110.9	9.3	12.3	0.75
49	24.3	8.2	110.3	9.2	13.0	0.75
50	24.6	6.9	76.6	6.4	20.4	0.85
51	24.8	5.8	62.7	5.2	18.2	3.00
52	24.5	7.3	96.6	8.1	12.8	1.50
53	24.4	8.6	111.6	9.3	13.0	0.75
54	24.6	8.6	111.9	9.3	12.9	0.85
55	24.7	8.6	111.8	9.3	13.1	0.85
56	24.6	8.5	112.4	9.4	13.2	0.85
57	24.7	8.6	112.5	9.4	13.0	0.75
Average	24.7	7 (7.8)	91	8	14	2
SD	0.2	1 (0.9)	20	2	2	1

distributions of the slope and $a(\lambda_0)$ in the whole lake, a geographical interpolation of the data was calculated and graphed (Fig. 10).

Water temperature, pH (pH units), DO saturation (DO, %), DO (DO, mg L^{-1}), conductance (C, µS cm^{-1}) and SDK depth (m) are presented in Tables 2–4 (SB, CB and NB, respectively).

The physical and chemical difference between basin measurements was examined using a *t*-test (Tables 5 and 6), which supports the geographical subdivision of the lake. The overestimation of the variance caused by spatial variation within each basin leads to the generation of an underestimation of the difference between basins but could be used to summarize the difference between basins.

The spatial representation of the UV and PAR irradiance attenuation coefficients can be used to examine some ecological aspects of the aquatic ecosystem. The spatial distributions of the DOM concentration coincide well with the distribution of UV attenuation coefficients. Using the spring sampling, the correlation

Table 5. *t*-Test analysis of the slopes and $a(\lambda_0)$ series of the SB, CB and NB. *P* is the probability associated to the Student *t*-Test.

	P
t-Test analysis on s	
SB *vs* CB	1×10^{-6}
CB *vs* NB	5×10^{-2}
NB *vs* SB	4×10^{-2}
t-Test analysis on $a(\lambda_0)$	
SB *vs* CB	4×10^{-8}
CB *vs* NB	0.17
NB *vs* SB	1×10^{-7}

Table 6. *t*-Test analysis on the physical and chemical measurement series between SB, CB and NB. The *t* values calculated without Stations 41–46 are presented in parentheses. *P* is the probability associated to the Student *t*-Test.

P	pH	DO (%)	DO	C	SDK
NB *vs* CB	9×10^{-3} (0.5)	6×10^{-3}	4×10^{-3}	3×10^{-3}	7×10^{-3}
NB *vs* SB	0.08 (0.001)	0.08	0.04	0.6	0.08
CB *vs* SB	1×10^{-5}	2×10^{-7}	0.1	1×10^{-9}	9×10^{-5}

between the measured UV attenuation coefficients and the concentration of DOM was determined using a nonlinear Eq. 4

$$K_{d,\lambda} = A_\lambda [DOM]^{B_\lambda} \quad (4)$$

The constants A_λ and B_λ were evaluated using the least squares method (Table 7).

The best correlation between the UV attenuation coefficients and the DOM was found at lower wavelengths (305 and 313 nm). The relationship between UV attenuation coefficients and DOM was found to be nearly linear ($B \approx 1$), considering B_λ together with its error (ΔB_λ) except for $K_{d,305}$. The values of B_λ are similar to those reported by Morris *et al.* (6) for dissolved organic carbon.

The spatial variations of both turbidity and fluorescence were found to be similar to the spatial distribution of the PAR attenuation coefficient in the spring survey. The relationship between these measurements was explored using a linear regression between variables (Table 8).

The difference between the DOM spectral parameters (s and $a(\lambda_0)$) has been reported to be related to the chemical properties and composition of the DOM fraction (37). The spatial distribution of the HA concentrations ([HA]), according to Mazzuoli *et al.* (30), as well as the ratio of [HA]:[DOM] is presented in Fig. 11 (data collected during the spring survey). Mazzuoli *et al.* (30) found that the ratio between the concentrations of FA ([FA]) and DOM was higher in areas where the [HA]:[DOM] ratio is lower. In our analysis, we found that $a(\lambda_0)$ was higher in the SB and in the southern part of CB (Fig. 10b). This spatial distribution was clearly related with DOM concentration (Fig. 8a). We found that the slopes in the central part of the CB present maximum values (Fig. 10a). Also, in this part of the lake, DOM was characterized by lower [HA] and lower ratio of [HA]:[DOM] (Fig. 11a,b). Assuming that the ratios of FA and the lower molecular weight fraction of DOM were higher in the CB, the difference in the slope values could be explained by a different spatial composition of the DOM. Consistent with del Vecchio and Blough (38), these distributions may have originated by a different level of photobleaching due to different exposure times of solar UV radiation. The CB was also characterized by a higher average value of pH (8.1 ± 0.4 pH units) and DO (saturation value, 107 ± 1% DO) with a lower average value of conductance (12.4 ± 0.3 μS cm^{-1}) with respect to the other basins. The UV attenuation coefficients in the NB during the spring season (Figs. 4b,d and 5b,d) were higher with respect to the CB. The DOM concentrations in these two basins (Fig. 8a) were similar. Turbidity, fluorescence (Fig. 8b,c) and K_{par} (Fig. 6b) were lower in the NB with respect to the CB. A possible explanation for this discrepancy may be found in relation to the chemical composition of DOM: HA is more efficient in absorbing 305, 313, 320 and 340 nm wavelengths. In the NB the [HA] and [HA]:[DOM] were higher than in the CB (Fig. 11a,b).

Table 7. Correlation between UV attenuation coefficients and DOM concentration according to Eq. 4. The errors were calculated with a confidence level of 99.9%. DF represents the degrees of freedom

$K_{d,\lambda}$	A_λ	ΔA_λ	B_λ	ΔB_λ	R^2 (%)	DF
305 nm	3.0	0.4	1.12	0.07	80	45
313 nm	3.2	0.4	1.05	0.07	74	63
320 nm	3.3	0.4	1.01	0.07	71	64
340 nm	2.9	0.4	0.97	0.07	69	72

CONCLUSIONS

The analysis of the spatial distribution of the UV and PAR attenuation coefficients demonstrated the high optical heterogeneity in the Iberà Lake. The spatial representation of the measurements was found to be a useful tool to describe the UV and visible environment of the lake and the related ecological aspects at local-scale resolution. Despite the relatively simple methodology, acceptable quality maps of physical, chemical and optical measurements are produced only when an adequate number of stations are used. The spatial resolution during the spring survey was 1.4/1 (number of sampling stations km^{-2}). Seasonal variations in the lake water quality will strongly affect the attenuation coefficients. The two sampling periods used in this investigation are insufficient to demonstrate seasonal trend, but correlation with hydrological (DOM) and biooptical characteristics (fluorescence and turbidity as indicators of phytoplankton and suspended solid) indicates that attenuation coefficients were sensitive to seasonal cycles.

The distribution of the optical measurements, the analysis of physical and chemical parameters and spectral proprieties of DOM support the division of the lake into three geographic basins.

The analysis of the spectral properties of the lake water by spectrophotometric methods was used to examine the geographical distribution of the concentration and composition of the DOM. In the SB, there is an inflow of DOM with relative high concentration of HA. In this study, a lower slope was also observed in this area. The NB has an input of DOM from a small river with a similar lower slope. These two rivers influence the spatial distribution of the slope in the lake. The difference between the two river water inflows, expressed by DOM fraction, is clear. There is a higher loading of DOM into the SB with respect to the NB, but the chemical composition, using slope information, is similar. This is confirmed by the analysis of the DOM fractions. In this lake, the areas with a lower [HA]:[DOM] ratio have a higher slope than areas with a higher [HA]:[DOM] ratio. Further analysis could be performed on the study of the residual between theoretical and measured absorbance of the DOM (Fig. 9). *In situ* experiments would be necessary to establish whether the slope values increase or decrease in the presence of photobleaching (39) and whether

Table 8. Linear correlation results between the $K_{d,par}$ (y) and turbidity (x, second row) and fluorescence (x, third row)

Y = ax + b	a	b	R^2	DF
Turbidity	3.1	0.96	0.71	65
Fluorescence	138	54	0.50	61

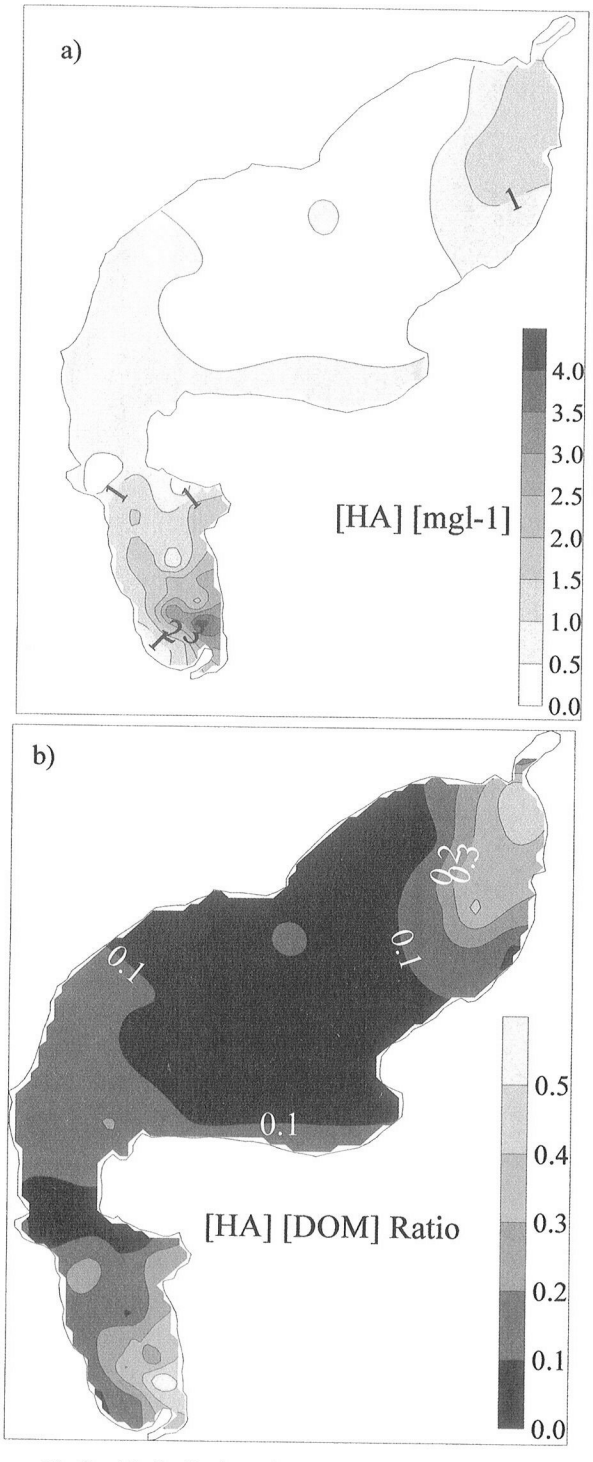

Figure 11. Spatial distribution of the concentration of (a) humic acid ([HA]) and (b) the ratio of [HA]:[DOM] measured during the spring survey.

bacterial activity has a primary or secondary effect on slope changes.

The spatial distribution of the UV attenuation was determined by two factors: the distribution of the DOM concentration and its composition. The spatial distribution measurements of $K_{d,par}$ were in good agreement with the fluorescence and turbidity distributions. The composition of the DOM (lower [HA], lower [HA]:[DOM] ratio and the probably higher [FA]:[DOM]) in the CB increases the metabolically available substrate for the microbial food web (40). In the same basin, higher values of $K_{d,par}$, fluorescence, turbidity, pH and DO were measured and conductance measurements were found to be at a minimum.

This analysis was aimed at determining the optical and ecological characteristics of the study ecosystem using a spatial resolution that is significantly higher than that used in other studies. The resulting maps of the lake's properties provided the possibility to examine the effect of solar radiation in different regions of the lake, especially in relation to the optical properties of DOM. They also make evident the role played by the rivers in the water quality of the aquatic ecosystem.

Acknowledgements—This work is supported through the European Commission Directorate General RTD INCO program (ERB I8 CT98 0262). This work is also supported through the Italian University and Research (MUIR) FIRB program (RBAU01CM44). The authors would like to thank Prof. Alessandro Donati of the University of Siena and Dr. Carmen Arena of the "Federico II" University of Naples, Italy. This research was also supported by the Italian interuniversity consortium CSGI.

REFERENCES

1. Ogura, N. and T. Hanya (1966) Nature of ultra-violet absorption of sea water. *Nature* **212**, 758.
2. Hader, D. P., H. D. Kumar, R. C. Smith and R. C. Worrest (1998) Effects on aquatic ecosystems. *J. Photochem. Photobiol. B: Biol.* **46**, 53–68.
3. Kirk, J. T. O. (1977) Use of a quanta meter to measure attenuation and underwater reflectance of photosynthetically active radiation in some inland and coastal south-eastern Australian waters. *Aust. J. Freshw. Res.* **28**, 9–21.
4. Scully, N. M. and D. R. S. Lean (1994) The attenuation of ultraviolet radiation in temperate lakes. In *Impact of UV-B Radiation on Pelagic Freshwater Ecosystems* (Edited by C. E. Williamson and H. E. Zagarese), pp. 135–144. Schweizerbart, Stuttgart, Germany.
5. Kirk, J. T. O., B. R. Hargreaves, D. P. Morris, R. B. Coffin, B. David, D. Frederickson, D. Karentz, D. R. S. Lean, M. P. Lesser, S. Mandronich, J. H. Morrow, N. B. Nelson and N. M. Scully (1994) Measurements of UV-B radiation in two freshwater lakes: an instrument intercomparison. In *Impact of UV-B Radiation on Pelagic Freshwater Ecosystems* (Edited by C. E. Williamson and H. E. Zagarese), pp. 71–99. Schweizerbart, Stuttgart, Germany.
6. Morris, D. P., H. Zagarese, C. E. Williamson, E. G. Balseiro, B. R. Hargreaves, B. Modenutti, R. Moller and C. Quimalinos (1995) The attenuation of solar UV radiation in lakes and the role of dissolved organic carbon. *Limnol. Oceanogr.* **40**(8), 1381–1391.
7. Nieke, B., R. Reuter, R. Heuermann, H. Wang, M. Babin and J. C. Therriault (1997) Light absorption and fluorescence properties of chromophoric dissolved organic matter (CDOM), in the St. Lawrence Estuary (Case 2 Water). *Continental Shelf Res.* **17**, 235–252.
8. Morel, A. and L. Prieur (1977) Analysis of variation in ocean colour. *Limnol. Oceanogr.* **22**, 709–722.
9. Huovinen, P. S., H. Pettila and M. R. Soimasuo (2003) Spectral attenuation of solar ultraviolet radiation in humic lakes in Central Finland. *Chemosphere* **51**, 205–214.
10. Laurion, I., M. Ventura, J. Catalan, R. Psenner and R. Sommaruga (2000) Attenuation of the ultraviolet radiation in mountain lakes: factors controlling the among- and within-lake variability. *Limnol. Oceanogr.* **45**(6), 1274–1288.
11. Vasilkov, A., N. Krotkov, J. Herman, C. McClain, K. Arrigo and W. Robinson (2001) Global mapping of underwater UV fluxes and DNA-weighted exposure using TOMS and SeaWifs data products. *J. Geophys. Res.* **106**, 27205–27219.
12. Amyot, M., G. Mierle, D. Lean and D. McQueen (1997) Effect of solar radiation on the formation of dissolved gaseous mercury in temperate lakes. *Geochim. Cosmochim. Acta* **61**, 975–987.
13. Beucher, C., P. Wong-Wah-Chung, C. Richard, G. Mailhot, M. Bolte and D. Cossa (2002) Dissolved gaseous mercury formation under UV

irradiation of unamended tropical waters from French Guyana. *Sci. Total Environ.* **290**, 131–138.
14. Bothwell, M. L., D. M. J. Sherbot and C. M. Pollock (1994) Ecosystem response to solar ultraviolet-b radiation: influence of trophic-level interactions. *Science* **265**, 97–100.
15. Karentz, D. (1994) Ultraviolet tolerance mechanisms in Antarctic marine organisms. Ultraviolet radiation in Antarctica: measurements and biological effects. *Antarct. Res. Ser.* **62**, 93–110.
16. Sommaruga, R. (2001) The role of solar UV radiation in the ecology of alpine lakes. *J. Photochem. Photobiol. B: Biol.* **62**, 35–42.
17. Yan, N. D., W. Keller, N. M. Scully, D. R. S. Lean and P. J. Dillon (1996) Increased UV-B penetration in a lake owing to drought-induced acidification. *Nature* **381**, 141–143.
18. Hakkinen, J., S. Pasanen and J. V. K. Kukkonen (2001) The effects of solar UV-B radiation on embryonic mortality and development in three boreal anurans (*Rana temporaria*, *Rana arvalis* and *Bufo bufo*). *Chemosphere* **44**, 441–446.
19. Smith, R. C. and K. S. Baker (1978) Penetration of UV-B and biologically effective dose-rates in natural waters. *Photochem. Photobiol.* **29**, 311–323.
20. Vincent, W. F. and P. J. Neale (2000) Mechanism of UV damage to aquatic organism. In *The Effects of UV Radiation on Marine Ecosystems* (Edited by S. J. de Mora, S. Demers and M. Vernet), pp. 149–204. Cambridge University Press, Cambridge.
21. Miller, R. L., M. Belz, C. De Castillo and R. Traska (2002) Determining CDOM absorption spectra in diverse coastal environments using a multiple pathlength, liquid core waveguide system. *Continental Shelf Res.* **22**, 1301–1310.
22. Warnock, R. E., W. W. C. Gieskes and S. Van Laar (1999) Regional and seasonal difference in light absorption by yellow substance in the Southern Bight of the North Sea. *Neth. J. Sea Res.* **42**, 169–178.
23. Conde, D., L. Aubriot and R. Sommaruga (2000) Changes in UV penetration associated with marine intrusions and freshwater discharge in a shallow costal lagoon of the Southern Atlantic Ocean. *Mar. Ecol. Prog. Ser.* **207**, 19–31.
24. Zagarese, H. E., M. Diaz, F. Pedroso, M. Ferraro, W. Cravero and B. Tartarotti (2001) Photodegradation of natural organic matter exposed to fluctuating levels of solar radiation. *J. Photochem. Photobiol. B: Biol.* **61**, 35–45.
25. Quian, J., K. Mopper and D. J. Kieber (2001) Photochemical production of the hydroxyl radical in Antarctic waters. *Deep-Sea Res.* **48**, 741–759.
26. Karentz, D. (1991) Ecological consideration of Antarctic ozone depletion. *Antarct. Sci.* **3**, 3–11.
27. Palenik, B., N. M. Price and F. M. M. Morel (1991) Potential effects of UV-B on the chemical environment of marine organism: a review. *Environ. Pollut.* **70**, 117–130.
28. Nieff, J. J. (1981) Panoramica Ecologico de Los Cuerpos de Agua del Nordeste Argentino. *Symposia, VI. Jornadas Argentinas de Zoologia*, pp. 115–151.
29. Bidoglio, G., D. Ferrari, E. Selli, F. Sena and G. Tamburini (1997) Humic acid binding of trivalent Tl and Cr studied by synchronous and time-resolved fluorescence. *Environ. Sci. Technol.* **31**, 3536–3543.
30. Mazzuoli, S., S. A. Loiselle, V. Hull, L. Bracchini and C. Rossi (2003) The analysis of the seasonal, spatial and compositional distribution of humic substances in a subtropical shallow lake. *Acta Hydrochim. Hydrobiol.* **31**, 461–468.
31. Peuravuori, J. and K. Pihlaja (1997) Molecular size distribution and spectroscopic properties of aquatic humic substances. *Anal. Chim. Acta* **337**, 133–149.
32. Hautala, K., J. Peuravuori and K. Pihlaja (2000) Measurement of aquatic humus content by spectroscopic analyses. *Water. Res.* **34**(1), 246–258.
33. Traina, S. J., J. Novak and N. H. Smeek (1990) An ultraviolet absorbance method of estimating the percent aromatic carbon content of humic acids. *J. Environ. Quant.* **19**, 151–153.
34. Bricaud, A., A. Morel and L. Prieur (1981) Absorption by dissolved organic matter of the sea (yellow substance) in the UV and visible domains. *Limnol. Oceanogr.* **26**, 43–53.
35. Markager, S. and W. F. Vincent (2000) Spectral light attenuation and the absorption of UV and blue light in natural waters. *Limnol. Oceanogr.* **45**(3), 642–650.
36. Stedmon, C. A., S. Markager and H. Kaas (2000) Optical properties and signature of choromophoric dissolved organic matter (CDOM) in Danish coastal waters. *Estuar. Coast. Shelf Sci.* **51**, 267–278.
37. Warnock, R. E., W. W. C. Gieskes and S. van Laar (1999) Regional and seasonal differences in light absorption by yellow substance in the Southern Bight of the North Sea. *J Sea Res.* **42**, 169–178.
38. Del Vecchio, R. and N. V. Blough (2002) Photobleaching of dissolved organic matter in natural waters: kinetics and modeling. *Mar. Chem.* **78**, 231–253.
39. Morris, D. P. and B. R. Hargreaves (1997) The role of photochemical degradation of dissolved organic carbon in regulating the UV transparency of three lakes on the Pocono Plateau. *Limnol. Oceanogr.* **42**, 239–249.
40. Zafiriou, O. C. (2002) Sunburnt organic matter: biogeochemistry of light-altered substrates. *Limnol. Oceanogr. Bull.* **11**(4), 69–74.